# High pressures pathway toward boron-based nanostructured solids

Remi Grosjean, Yann Le Godec, Simon Delacroix, Guillaume Gouget, Patricia Beaunier, Ovidiu Ersen, Dris Ihiawakrim, Oleksandr O Kurakevych, Corinne Chanéac, David Portehault

# High pressures pathway toward boron-based nanostructured solids

Rémi Grosjean,[a,b] Yann Le Godec,[b,*] Simon Delacroix,[a,b] Guillaume Gouget,[a] Patricia Beaunier,[c] Ovidiu Ersen,[d] Dris Ihiawakrim,[d] Oleksandr O. Kurakevych,[b] Corinne Chanéac,[a] David Portehault[a,*]

[a.] Sorbonne Université, CNRS, Collège de France, Laboratoire Chimie de la Matière Condensée de Paris, LCMCP, 4 Place Jussieu, F-75005 Paris, France. E-mail: david.portehault@sorbonne-universite.fr

[b.] Sorbonne Université, CNRS, MNHN, IRD, Institut de Minéralogie, de Physique des Matériaux et de Cosmochimie, IMPMC, 4 Place Jussieu, F-75005 Paris, France. E-mail: yann.le_godec@sorbonne-universite.fr

[c.] Sorbonne Université, CNRS, Laboratoire de Réactivité de Surface, LRS, 4 Place Jussieu, F-75005 Paris, France

[d.] Institut de Physique et Chimie des Matériaux de Strasbourg, CNRS-ULS UMR 7504, 23 rue du Loess, 67087 Strasbourg, France.

Electronic Supplementary Information (ESI) available: Experimental details, FTIR data, XPS, XRD and TEM characterization of a $CaB_6/CaB_2O_4$ nanocomposite. See DOI: 10.1039/x0xx00000x

**Inorganic nanocomposites made of an inorganic matrix containing nanoparticle inclusions provide materials of advanced mechanical, magnetic, electrical properties and multifunctionality. The range of compounds that can be implemented in nanocomposites is still narrow and new preparation methods are required to design such advanced materials. Herein we describe how the combination of nanocrystal synthesis in molten salts, with subsequent heat treatment at pressures in the GPa range, gives access to a new family of boron-based nanocomposites. With the case studies of $HfB_2$/β-$HfB_2O_5$ and $CaB_6/CaB_2O_4$ (IV), we demonstrate by X-Ray Diffraction and thorough (Scanning) Transmission Electron Microscopy the crystallization of borate matrices into rare compounds and unique nanostructured solids, while metal boride nanocrystals remain dispersed in the matrix and maintain small sizes below 30 nm, thus demonstrating a new multidisciplinary approach toward nanoscaled heterostructures.**

## Introduction

Inorganic nanocomposites are made of an inorganic matrix that contains nanoparticle inclusions to target original mechanical, magnetic, electrical properties and multifunctionality.[1–5] The production methods known to yield ceramic matrix nanocomposites consist mostly in two approaches: either embedding preformed nanoparticles into matrices, or precipitating the inclusions directly in the matrix.[2,3] These techniques are restricted to simple oxide and nitride matrices. To push further the opportunities given by these complex systems, the range of compounds to be implemented in nanocomposites must be widened. We present herein a third route based on the crystallization of the matrix around nanoparticles in extreme conditions, in order to combine crystalline matrices and nanoparticles of rare structures and compounds.

High pressures and temperatures (HP-HT) ranging from 1 to 20 GPa and from 500 to 1500 °C are a realm of opportunities to synthesize crystalline materials not reachable at pressures close to the atmospheric one.[6–9] Such HP-HT ranges are compatible with large scale industrial productions.[10] But to yield nanocomposites, nanoscaled inclusions should survive such extreme conditions, thus questioning the behavior of nanostructured materials under HP-HT treatment.

Current HP studies on nanoparticles deal with two families of solids: (1) metal oxides by applying HP only and no heating,[11–14] (2) light element B, C, or N-based non-oxides that crystallize only under both HP and HT.[7,15–17] In the latter case, nanostructuration increases hardness toward ultrahard materials (*e.g.* nanostructured diamond or *c*-BN).[7,17–24] Overall, all previous studies on nanostructured materials under extreme conditions focused on single phase systems, phases that could be obtained at room pressure, or nanocomposites made of well-known high pressure solid state phases. A new preparation method of nanocomposites with high control over the size and the composition of the nanoinclusions, and which could provide access to complex solids, would open new perspectives for the production of original nanocomposites with controlled properties.

Here, we focus as a case study on metal borate matrices containing as inclusions nanocrystals of metal-boron compounds, so-called metal borides. Borates have not been reported as nanostructured materials. In the bulk form, they show unique properties as boron sources,[25] glass modifiers,[25] Li-ion battery electrodes,[26] ionic conductors[27] and materials for non-linear optics.[25] Combining borates with nanoscaled borides could bring some distinctive properties of boride nanocrystals: high electrical and thermal conductivity, hard/soft magnetic properties, very high hardness and catalytic properties.[28–31] HP conditions are among the most versatile methods[25,27,32–36] used to synthesize borates with new crystal structures, unachievable at close-to-room pressure.[37–45] Hence, HP-derived nanocomposites made of borate matrices and metal boride nano-inclusions should pave the way to a large range of new multifunctional materials.

In this work we propose a multidisciplinary approach merging nanomaterials chemistry with high pressure physics. We synthesize nanocrystals of metal borides, precipitated in inorganic molten salts,[28,46–49] and then treat these nanoscaled precursors under high pressure conditions, to trigger the crystallization of HP borate matrices around the nanocrystals. Both $HfB_2$/β-$HfB_2O_5$ and $CaB_6$/$CaB_2O_4$-(IV) nanocomposites are discussed, as a proof-of-concept of this method.

## Results and discussion

The nanoscaled precursors for subsequent HP-HT transformations consist in boride nanocrystals embedded into an amorphous boron-rich matrix. Their synthesis was performed by precipitation in the molten eutectic mixture LiCl:KCl, which can be heated up to 900 °C at room pressure.[46,47] The resulting particles[28,46] are surrounded by an amorphous matrix, which was shown[28,46] to consist mainly in boron slightly oxidized, from the exposure of powders to water and air during washing. To ensure evolution under HP-HT of the amorphous matrix toward borates and not boron polymorphs, the powders were exposed to air for 7 days to allow oxidation of the boron matrix. Vibrations characteristic of B-O bonds are evidenced at 1350 $cm^{-1}$ on the infrared spectra (Supplementary Information **Figure S1)**.

The case-study of hafnium diboride $HfB_2$ is discussed first. XRD (**Figure 1**) shows that $HfB_2$ is obtained as a pure crystalline phase. The crystallite size is ca. 8 nm from the Scherrer formula. It is consistent with Transmission Electron Microscopy (TEM, **Figure 2a**), which exhibits 5 to 10 nm strongly contrasted nanocrystals with lattice fringes (FFT, **Figure 2a** insert) indexed along the $HfB_2$ structure. The single-crystal particles are isotropic. This molten salt method is ideal to yield the smallest particle size reported for crystalline $HfB_2$ and other borides.[28] X-ray Photoelectron Spectroscopy (XPS) (**Figure S2** with detailed discussion in SI) confirms that the matrix embedding the nanocrystals is made of oxidized boron, with characteristic B1s peaks at 192.4 and 190.0 eV, in addition to the 186.6 eV peak typical for $HfB_2$ and 187.9 eV for elemental boron.[50] The nature of the matrix was also assessed by mean of Scanning Transmission Electron Microscopy combined to High Angle Annular Dark Field detection (STEM-HAADF) for atomic number-contrast. The comparison of bright and dark field images (**Figure 2a, b**) shows contrasted crystalline $HfB_2$ particles. The matrix is heterogeneous in brightness, with *ca.* 2 nm clusters contrasting (empty arrows in **Figure 2a, b**) with the rest of the matrix. These bright areas highlight the presence of hafnium within the matrix. The thickness of the amorphous phase comprising hafnium clusters and amorphous oxidized boron is about 3 nm. Consequently,

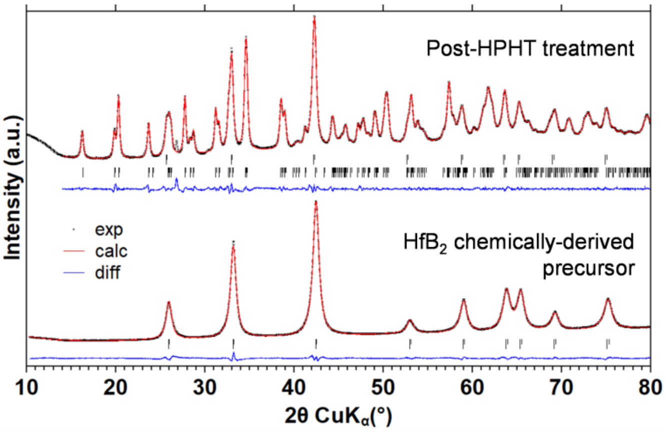


**Figure 1. XRD powder patterns** of the initial $HfB_2$-based precursor and of the $HfB_2$/$HfB_2O_5$ nanocomposite obtained after treatment at 5 GPa and 1200 °C. Le Bail refinements were performed according to $HfB_2$ and β-$HfB_2O_5$ structures with ICSD reference cards 30422 and 417031, respectively.

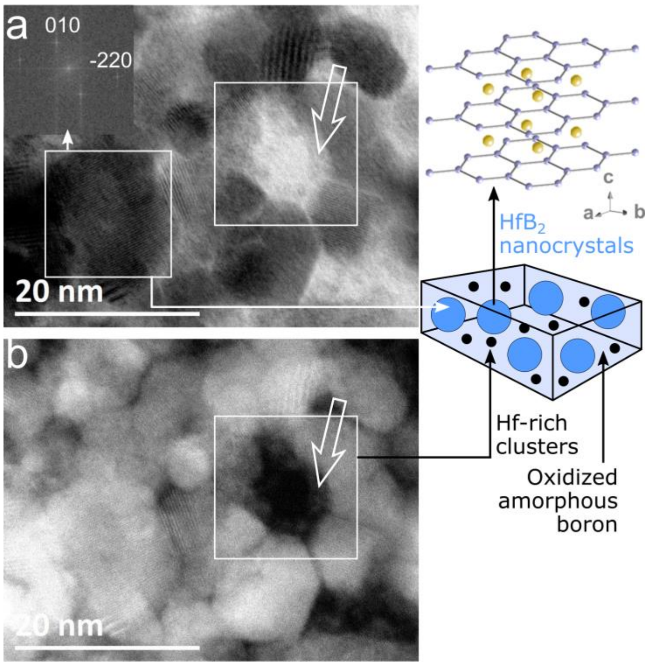


**Figure 2. TEM study of the nanoscaled hafnium-based precursor.** (a) Bright field STEM image, insert: Fast Fourier Transform (FFT) of the squared zone on one nanocrystal, indexed on the $HfB_2$ structure (yellow: Hf atoms, gray: B atoms). (b) Corresponding STEM-HAADF Z-contrast image evidencing Hf-rich clusters. The empty arrows in (a) and (b) point at *ca.* 2 nm Hf-rich clusters. Scheme describing the initial material's nanocomposite structure according to XRD and TEM.

between two adjacent nanocrystals, a gap smaller than 10 nm is filled with oxidized amorphous boron doped with Hf atoms and clusters. The system is best described as "nano-cookie": the boride nanocrystals are included within the amorphous nanostructured matrix. Therefore, both components are nanostructured: the crystalline phase as nanoscale inclusions and the amorphous matrix made of nanoscale walls between the crystalline inclusions (**Figure 2**).

The oxidized composite was placed in a large volume high pressure device (**Figure 3**): a Paris-Edinburgh cell assembly, producing 1.5 mm diameter by 1-2 mm height pellets after HP-HT treatment. The sample was pressed at 5 GPa and heated to 1200 °C in 45 min, followed by a 90 min dwell time. After HP-

HT treatment, the sample was quenched by cooling down to room temperature (ca. 1 min) and then slowly releasing the pressure over 12 h. The assembly was opened in air to recover the samples. For the hafnium-based system, the XRD pattern (**Figure 1**) first shows that hafnium diboride is conserved upon HP-HT treatment. The Scherrer crystallite size evidences preservation of the nanoscale although slight particle growth occurred, with average size of 25 nm. XRD also indicates crystallization of another phase identified as hafnium borate β-$HfB_2O_5$. This phase was first prepared by Knyrim and Huppertz from $HfO_2$ and $B_2O_3$ at 7.5 GPa and 1100 °C.[41] To our knowledge, we provide in this report the second occurrence of this crystalline ternary hafnium borate, and the first case of nanostructured β-$HfB_2O_5$. Refined cell parameters of $HfB_2$ and $HfB_2O_5$ were close to the reported values: a = b = 3.1457(4) Å, c = 3.4733(6) Å for $HfB_2$ prior to the HP-HT treatment; a = b = 3.1479(6) Å, c = 3.4826(10) Å for $HfB_2$ and a = 4.3904(7) Å, b = 6.9137(10) Å, c = 8.9953(17) Å, β = 90.728(10) ° for $HfB_2O_5$ in the post-HP-HT sample.

STEM images (**Figure 4a, b**) and particle size distributions (**Figure 4b insert**) confirm the limited grain growth: the particle size does not exceed 30 nm after a treatment at 1200 °C. The matrix is crystallized into β-$HfB_2O_5$ evidenced by characteristic lattice distances (**Figure 4c, d**), in agreement with XRD. Thus, the amorphous matrix undergoes crystallization upon HP-HT. The interparticle gap is preserved (**Figure 4a, b, d**), leading to nanostructured $HfB_2$/β-$HfB_2O_5$ composite monoliths, which may be described again as "nano-cookies": a crystalline β-$HfB_2O_5$ matrix embedding nano-inclusions of $HfB_2$ and containing nanoscaled walls separating the inclusions. The matrix thus remains confined between these inclusions.

The overall evolution of the sample and the synthesis approach are schematized **Figure 5**. The HP-HT treatment preserves the metal boride nanocrystals with limited grain growth, while the treatment mostly affects the matrix that crystallizes into a rare borate phase but keeps its structuration around the nanocrystals. Remarkably, up to now only scarce reports have described the synthesis of nanostructured inorganic materials under HP-HT conditions.[11–14,51] Indeed, such treatments usually yield reduced interfaces by large crystal growth. Our striking result arises from two kinetic factors. First, high pressure limits atomic diffusion,[52] thus increasing the activation barrier necessary for grain growth. Second, high pressure is also likely to restrain particle migration within the matrix they are embedded in. In the case-study shown here, hafnium atoms initially present in the amorphous boron-rich matrix yield crystallization of β-$HfB_2O_5$ upon HP-HT treatment.

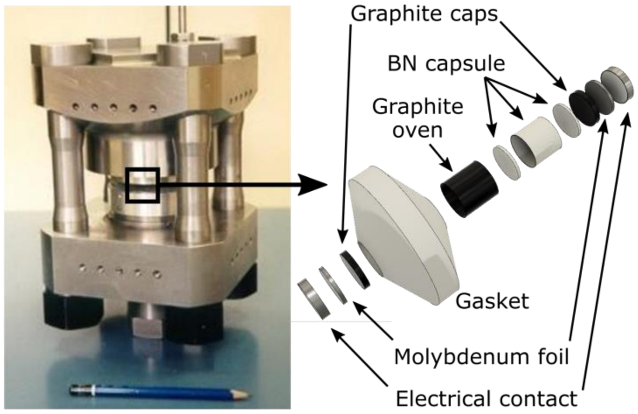


**Figure 3. HP-HT set-up:** picture of a Paris-Edinburgh press and zoom (schematized) on the cell assembly. The sample is filled in the BN capsule. The diameter of the oven is initially 2 mm, 1.5 mm after HTP-HT treatment.

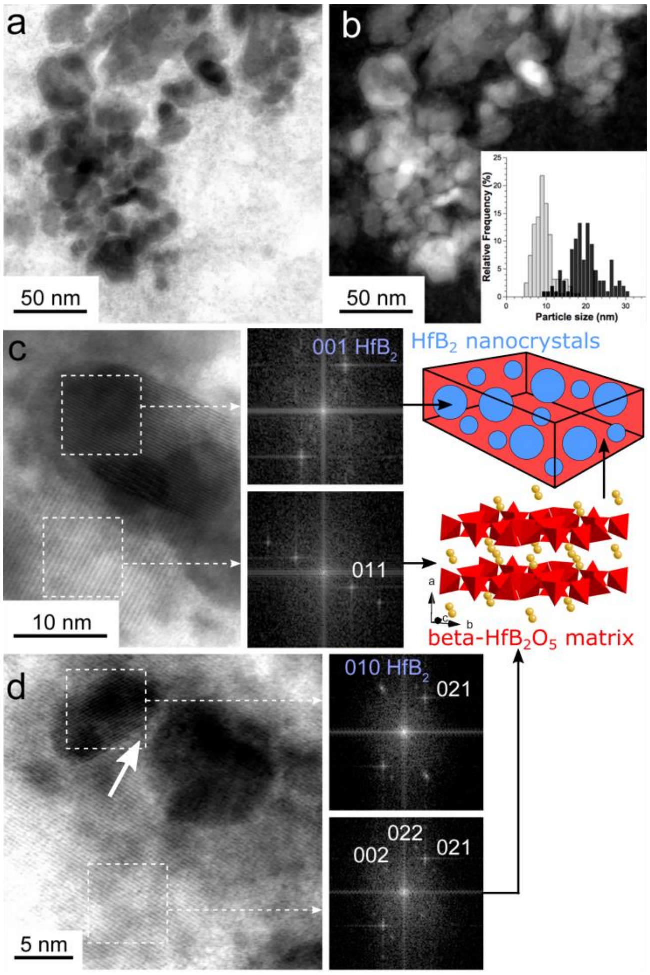


**Figure 4. TEM study of the $HfB_2$ nanocrystal-based nanocomposite obtained after HP-HT treatment:** (a) bright field STEM image, (b) corresponding STEM-HAADF image with particle size distribution of the initial $HfB_2$ nanocrystals (light gray) and the $HfB_2$ nanocrystals observed after HP-HT treatment (dark gray). (c), (d) STEM images and corresponding Fast Fourier Transforms indexed along the $HfB_2$ (blue) and β-$HfB_2O_5$ (white) structures (yellow: Hf atoms, red: $BO_4$ tetrahedra). The white arrow in (d) shows an interparticle gap.

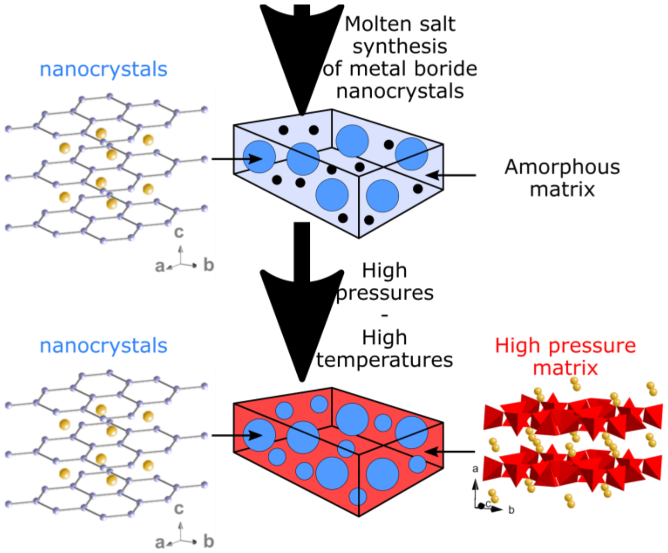


**Figure 5. Scheme of the molten salt synthesis/high pressure-high temperature transformation approach** toward new boron-based nanocomposites.

To demonstrate the generalization of the approach, we have explored another boride/borate system, relying on $CaB_6$ nanocrystals (Supplementary Information and **Figure 6**). The initial ~15 nm crystalline nanoparticles embedded in an amorphous boron-rich matrix (**Figure 6** and **Figure S3**) have been prepared in molten salts.[46] After HP-HT treatment (5 GPa, 1200 °C), the $CaB_6$ nanocrystals have only slightly grown, with diameter maintained below 30 nm (**Figure S4**). The matrix crystallized into the $CaB_2O_4$ (IV) phase (**Figure 6** and **Figures S3, S4**) that was reported only once[53] and as bulk material. Again, we report the first occurrence of a nanostructured material based on this high pressure phase, as well as the first nanocomposite with such an HP solid as matrix.

## Conclusions

To conclude, we have shown the original combination of chemically-derived metal boride nanocrystals with HP-HT treatments to prepare innovative nanocomposites by high pressure crystallization of ternary borates. Nanostructuration is preserved upon crystallization of the matrix at extreme HP conditions, with the size of the nano-inclusions not exceeding 30 nm at pressures as high as 5 GPa. These results validate this new approach combining solution-phase synthesis of inorganic nanomaterials and high pressures to yield nanocomposites made of phases not reachable at ambient conditions. Especially, the method benefits from the ability of molten salt synthesis to prepare single-phase metal boride nanocrystals in order to reach nanocomposites well controlled from the compositional viewpoint.[28,46,47,54] The resulting materials establish a new family of heterostructures built on HP solids. They provide an intimate combination of metallic ($HfB_2$) or insulating ($CaB_6$) nano-inclusions with rare insulating ceramic compounds. This approach paves the way to advanced mechanical, electrical, thermal and optical properties.

## Conflicts of interest

There are no conflicts of interest to declare.

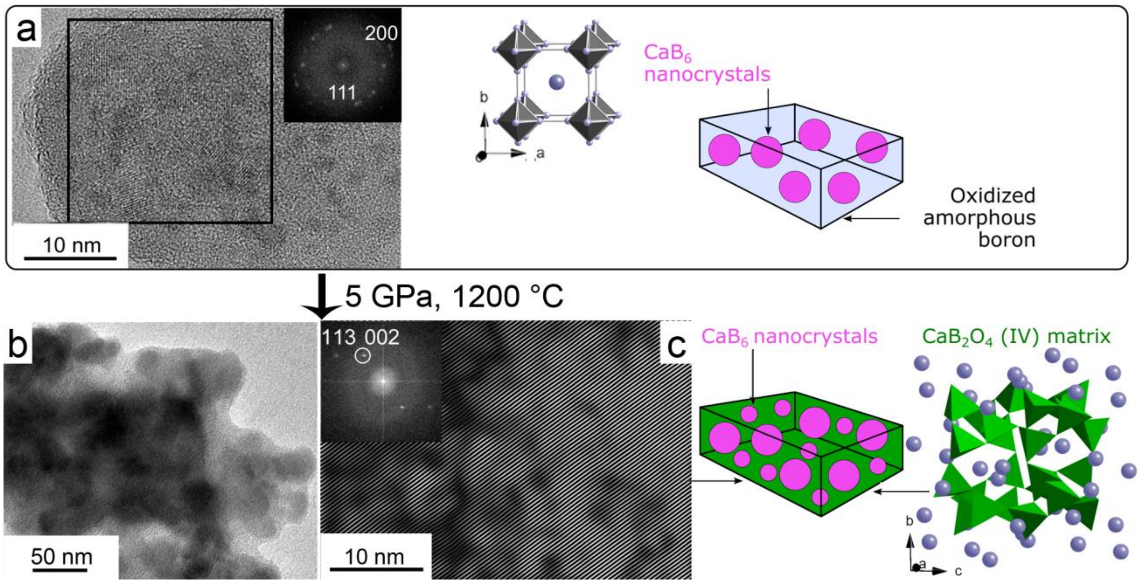


**Figure 6. TEM study of the $CaB_6$ nanocrystal-based nanocomposite before (a and corresponding scheme with $CaB_6$ structure (blue: Ca atom, gray: $B_6$ octahedra)) and after HP-HT crystallization (b, c and corresponding scheme with $CaB_2O_4$ (IV) structure (blue: Ca atoms, green: $BO_4$ tetrahedra)):** (a) TEM image of the initial $CaB_6$-amorphous matrix composite, (b) TEM image and (c) Fourier-Filtered image of an HRTEM micrograph highlight the good crystallinity of the crystalline $CaB_2O_4$ (IV) matrix.

## Acknowledgements

Christophe Calers is acknowledged from the Centre of Institute of Materials of Paris Centre is acknowledge for XPS measurements. The authors thank the Centre National de la Recherche Scientifique, its Energy Unit and French state funds managed by the ANR within the Investissements d'Avenir programme ANR-11-IDEX-0004-02, more specifically within the Cluster of Excellence MATISSE, for funding. The Agence Nationale de la Recherche (project ANR-2011-BS08-018), Sorbonne Universités-UPMC, Collège de France and the METSA (Microscopie Electronique et Sonde Atomique) network are also acknowledged for financial support.

## Notes and references

1 P. M. Ajayan, L. S. Schadler and P. V. Braun, Eds., *Nanocomposite science and technology*, Wiley-VCH, Weinheim, Germany, 2003.
2 M. C. Bechelany, V. Proust, C. Gervais, R. Ghisleni, S. Bernard and P. Miele, *Adv. Mater.*, 2014, **26**, 6548–6553.
3 G. Mera, M. Gallei, S. Bernard and E. Ionescu, *Nanomaterials*, 2015, **5**, 468–540.
4 H. Zeng, J. Li, J. P. Liu, Z. L. Wang and S. Sun, *Nature*, 2002, **420**, 395–398.
5 A. Eftekhari, *J. Power Sources*, 2017, **343**, 395–411.
6 O. O. Kurakevych, T. a. Strobel, D. Y. Kim, T. Muramatsu and V. V. Struzhkin, *Cryst. Growth Des.*, 2013, **13**, 303–307.
7 V. L. Solozhenko, O. O. Kurakevych and Y. Le Godec, *Adv. Mater.*, 2012, **24**, 1540–1544.
8 A. R. Oganov, J. Chen, C. Gatti, Y. Ma, Y. Ma, C. W. Glass, Z. Liu, T. Yu, O. O. Kurakevych and V. L. Solozhenko, *Nature*, 2009, **457**, 863–867.
9 V. L. Solozhenko, O. O. Kurakevych, D. Andrault, Y. Le Godec and M. Mezouar, *Phys. Rev. Lett.*, 2009, **102**, 15506.
10 P. F. McMillan, *Nat. Mater.*, 2002, **1**, 19–25.
11 E. J. Gonzalez, B. Hockey and G. J. Piermarini, *Mater. Manuf. Process.*, 1996, **11**, 951–967.
12 J. S. Olsen, L. Gerward and J. Z. Jiang, *High Press. Res.*, 2002, **22**, 385–389.
13 H.-C. Chang, J.-C. Jiang, M.-H. Kuo, D.-T. Hsu and S. H. Lin, *Phys. Chem. Chem. Phys.*, 2015, **17**, 21143–21148.
14 B. Liu, M. Yao, B. Liu, Z. Li, R. Liu, Q. Li, D. Li, B. Zou, T. Cui and Z. Chen, *J. Phys. Chem. C*, 2011, 4546–4551.
15 A. Nagakubo, H. Ogi, H. Sumiya and M. Hirao, *Appl. Phys. Lett.*, 2014, **105**, 81906.
16 B. Liang, Y. Xie, W. Li, W. Wu and X. Zhang, *J. Phys. D. Appl. Phys.*, 2008, **41**, 195010.
17 N. Dubrovinskaia, V. L. Solozhenko, N. Miyajima, V. Dmitriev, O. O. Kurakevych and L. Dubrovinsky, *Appl. Phys. Lett.*, 2007, **90**, 1–4.
18 T. Irifune, A. Kurio, S. Sakamoto, T. Inoue and H. Sumiya, *Nature*, 2003, **421**, 599–600.
19 N. Dubrovinskaia, L. Dubrovinsky, F. Langenhorst, S. Jacobsen and C. Liebske, *Diam. Relat. Mater.*, 2005, **14**, 16–22.
20 Y. Zhao, D. W. He, L. L. Daemen, T. D. Shen, R. B. Schwarz, Y. Zhu, D. L. Bish, J. Huang, J. Zhang, G. Shen, J. Qian and T. W. Zerda, *J. Mater. Res.*, 2002, **17**, 3139–3145.
21 V. L. Solozhenko, D. Andrault, G. Fiquet, M. Mezouar and D. C. Rubie, *Appl. Phys. Lett.*, 2001, **78**, 1385–1387.
22 Y. Tian, B. Xu, D. Yu, Y. Ma, Y. Wang, Y. Jiang, W. Hu, C. Tang, Y. Gao, K. Luo, Z. Zhao, L.-M. Wang, B. Wen, J. He and Z. Liu, *Nature*, 2013, **493**, 385–8.
23 V. L. Solozhenko, S. N. Dub and N. V Novikov, *Diam. Relat. Mater.*, 2001, **10**, 2228–2231.
24 R. H. Wentorf, *J. Chem. Phys.*, 1961, **34**, 809.
25 H. Huppertz and D. A. Keszler, in *Encyclopedia of Inorganic and Bioinorganic Chemistry*, Wiley, 2014, pp. 1–12.
26 A. Yamada, N. Iwane, Y. Harada, S. Nishimura, Y. Koyama and I. Tanaka, *Adv. Mater.*, 2010, **22**, 3583–3587.
27 F. Strauss, G. Rousse, D. Alves Dalla Corte, M. Ben Hassine, M. Saubanère, M. Tang, H. Vezin, M. Courty, R. Dominko and J.-M. Tarascon, *Phys. Chem. Chem. Phys.*, 2016, **18**, 14960–14969.
28 S. Carenco, D. Portehault, C. Boissière, N. Mézailles and C. Sanchez, *Chem. Rev.*, 2013, **113**, 7981–8065.
29 X. H. Ji, Q. Y. Zhang, J. Q. Xu and Y. M. Zhao, *Prog. Solid State Chem.*, 2011, **39**, 51–69.
30 T. Mori, *J. Phys. Conf. Ser.*, 2009, **176**, 12036.
31 J. B. Levine, S. H. Tolbert and R. B. Kaner, *Adv. Funct. Mater.*, 2009, **19**, 3519–3533.
32 H. Kouta, Y. Kuwano, K. Ito and F. Marumo, *J. Cryst. Growth*, 1991, **114**, 676–682.
33 J. Brinker, *Silica Glass and its Application*, Elsevier, 1991, vol. 11.
34 N. Venkatasubramanian, B. Wade, P. Desai, A. S. Abhiraman and L. T. Gelbaum, *J. Non. Cryst. Solids*, 1991, **130**, 144–156.
35 H. G. Snowman, *Sol-gel technology for thin films, fibers, preforms, electronics, and specialty shapes*, 1988.
36 L. N. Demianets, *Prog. Cryst. Growth Charact. Mater.*, 1991, **21**, 299–355.
37 H. Huppertz, *Chem. Commun.*, 2011, **47**, 131–40.
38 H. Emme and H. Huppertz, *Acta Crystallogr. Sect. C*, 2005, **3**, 29–31.
39 H. Emme and H. Huppertz, 2002, **204**, 69451.
40 H. Emme and H. Huppertz, *Chemistry*, 2003, **9**, 3623–33.
41 J. S. Knyrim and H. Huppertz, *J. Solid State Chem.*, 2007, **180**, 742–748.
42 G. Sohr, N. Ciaghi, M. Schauperl, K. Wurst, K. R. Liedl and H. Huppertz, *Angew. Chemie Int. Ed.*, 2015, **5**, n/a-n/a.
43 H. Emme, M. Valldor, R. Po and H. Huppertz, *Chem. Mater.*, 2005, **17**, 2707–2715.
44 H. Huppertz and B. von der Eltz, *J. Am. Chem. Soc.*, 2002, **124**, 9376–9377.
45 J. S. Knyrim, F. Roessner, S. Jakob, D. Johrendt, I. Kinski, R. Glaum and H. Huppertz, *Angew. Chem. Int. Ed.*, 2007, **46**, 9097–90100.
46 D. Portehault, S. Devi, P. Beaunier, C. Gervais, C. Giordano, C. Sanchez and M. Antonietti, *Angew. Chem. Int. Ed.*, 2011, **50**, 3262–3265.
47 G. Gouget, P. Beaunier, D. Portehault and C. Sanchez, *Faraday Discuss.*, 2016, **191**, 511–525.
48 B. Terlan, A. Levin, F. Börrnert, F. Simon, M. Oschatz, M. Schmidt, R. Cardoso-Gil, T. Lorenz, I. Baburin, J.-O. Joswig and A. Eychmueller, *Chem. Mater.*, 2015, **27**, 5106–5115.
49 B. Terlan, A. A. Levin, F. Börrnert, J. Zeisner, V. Kataev, M. Schmidt and A. Eychmueller, *Eur. J. Inorg. Chem.*, 2016, **2016**, 3460–3468.
50 G. Mavel, J. Escard, P. Costa and J. Castaing, *Surf. Sci.*, 1973, **35**, 109–116.
51 S. Dogra, N. D. Sharma, J. Singh, H. K. Poswal, S. M. Sharma

and A. K. Bandyopadhyay, *High Press. Res.*, 2011, **31**, 292–303.

52 Helmut Mehrer, *Diffusion in Solids*, Springer Berlin Heidelberg, Berlin Heidelberg, 2007.

53 M. Marezio, J. P. Remeika and P. D. Dernier, *Acta Crystallogr. Sect. B Struct. Crystallogr. Cryst. Chem.*, 1969, **25**, 965–970.

54 G. Gouget, D. P. Debecker, A. Kim, G. Olivieri, J.-J. Gallet, F. Bournel, C. Thomas, O. Ersen, S. Moldovan, C. Sanchez, S. Carenco and D. Portehault, *Inorg. Chem.*, 2017, **56**, 9225–9234.

# Supplementary Information

## High pressures pathway toward boron-based nanostructured solids

Rémi Grosjean,[a,b] Yann Le Godec,[b,*] Simon Delacroix,[a,b] Guillaume Gouget,[a] Patricia Beaunier,[c] Ovidiu Ersen,[d] Dris Ihiawakrim,[d] Oleksandr O. Kurakevych,[b] Corinne Chanéac,[a] David Portehault[a,*]

[e.] *Sorbonne Université, CNRS, Collège de France, Laboratoire Chimie de la Matière Condensée de Paris, LCMCP, 4 Place Jussieu, F-75005 Paris, France*
[f.] *Sorbonne Université, CNRS, MNHN, IRD, Institut de Minéralogie, de Physique des Matériaux et de Cosmochimie, IMPMC, 4 Place Jussieu, F-75005 Paris, France*
[g.] *Sorbonne Université, CNRS, Laboratoire de Réactivité de Surface, LRS, 4 Place Jussieu, F-75005 Paris, France*
[h.] *Institut de Physique et Chimie des Matériaux de Strasbourg, CNRS-ULS UMR 7504, 23 rue du Loess, 67087 Strasbourg, France.*

### MATERIALS AND METHODS

### FIGURES

## MATERIALS AND METHODS

*Synthesis of the nanoscaled precursors.* Before heating, all powders were handled into an argon-filled glovebox. Anhydrous $HfCl_4$ (Alfa Aesar, 99.9 %), $CaCl_2$ (Alfa Aesar, 99.9 %) and $NaBH_4$ (Alfa Aesar, 98 %) were used as received. Prior to synthesis, LiCl and KCl (Aldrich) were mixed at the eutectic composition LiCl:KCl = 45:55 wt% and finely ground in a mortar. The resulting mixture was evacuated at 200 °C for 4 days and transferred into the glovebox. Before heating, anhydrous metal chlorides, sodium borohydride and the eutectic salt mixture LiCl:KCl (2.5 g) were finely ground together with a Retsch MM400 ballmiller (airtight vials of 50 mL, one steel ball of 62.3 g and a diameter of 23 mm) for 2 min at 20 Hz. The mixture was transferred into a glassy carbon crucible which was then heated under argon flow in a tube oven at 10 °C $min^{-1}$. For $HfB_2$, 1 mmol of hafnium (IV) chloride and 4 mmol of sodium borohydride were used. The reaction medium was heated at 900 °C for 4 h. For $CaB_6$, 1 mmol of calcium (II) chloride and 8 mmol of sodium borohydride were used. The reaction medium was heated at 800 °C for 4 h. After cooling, the metal boride powders were recovered by dissolution of the frozen eutectic in deionized water and four washing-centrifugation cycles (in 10 mL polycarbonate centrifugation tubes, at 16500 rpm for 20 min), then dried under vacuum at 60 °C overnight.

*Characterizations.*
The precursors and products were characterized with a Bruker D8 X**-ray diffractometer** operating in the Bragg-Brentano reflection mode equipped with a nickel filter to select the Cu-$K_\alpha$ radiation. The data were collected in the 2θ = 10-80 ° range with 0.05 ° steps. For samples recovered after HP-HT treatment, crystalline silicon low-background sample holders from Bruker were used for XRD analysis.

The morphology and the average particle size of the samples were analysed by **transmission electron microscopy (TEM)** using a Tecnai spirit G2 apparatus ($LaB_6$, operating at 120 kV). HRTEM analyses were performed on a JEOL JEM 2011 ($LaB_6$, operating at 200 kV) apparatus at the Microscopy Centre of Institute of Materials of Paris Centre (IMPC), Sorbonne Universités-UPMC, Paris. **The STEM-HAADF and STEM-DF** observations were performed on a JEOL 2100 F operating at 200 kV and equipped with aberration correction on the electronic probe at the Institut de Physique et Chimie de la Matière de Strasbourg.

**XRD and high resolution (S)TEM** data were indexed along the ICSD reference cards 30422, 196516, 417031 and 23241 for $HfB_2$, $CaB_6$, $\beta$-$HfB_2O_5$ and $CaB_2O_4$ (IV), respectively. Le Bail refinements of XRD data were performed on JANA2006 software (Petrícek, V.; Dušek, M.; Palatinus, L. Crystallographic Computing System JANA2006: General Features. *Zeitschrift fur Krist.* **2014**, *229* (5), 345–352). All samples for (S)TEM were prepared by evaporating a drop of diluted suspension in ethanol on a carbon-coated copper grid. For infrared spectroscopy, a Perkin-Elmer spectrum 400 FT-IR apparatus equipped with ATR FT-IR was used.

For **X-ray photoelectron spectroscopy (XPS)**, the spectra were recorded on an Omicron Technology apparatus at the IMPC. It was equipped with a hemispheric analyzer (SPECS) and an aluminum cathode with an Al Kα monochromator. The analysis of the data was performed on CasaXPS software. The spectra were calibrated according to the C 1s signal at 285.0 eV. Shirley background type was chosen in Hf 4f region and linear background type in B 1s and O 1s regions. Binding energy and full width at half maximum (BE, eV; FWHM, eV) of contributions are (i) in the Hf 4f region : Hf-B ($4f_{7/2}$)(14.3, 0.9), ($4f_{5/2}$)(16.0, 0.9) and $Hf^{(IV)}$ ($4f_{7/2}$)(17.4, 1.4) ($4f_{5/2}$)(19.1, 1.4) (ii) in the B 1s region: B-Hf (186.6, 0.9), $B^{(0)}$ (188.0, 1.5), B-O (189.7, 1.5), $BO_3$ (192.3, 1.6) and (iii) in the O 1s region: (531.9, 2.3). In the Hf 4f region, constraints were imposed between contributions due the $4f_{7/2}$-$4f_{5/2}$ spin-orbit splitting: BE($4f_{5/2}$) = BE($4f_{7/2}$) + 1.7 eV ; Area($4f_{5/2}$) = 0.75 Area($4f_{7/2}$).

**FIGURES**

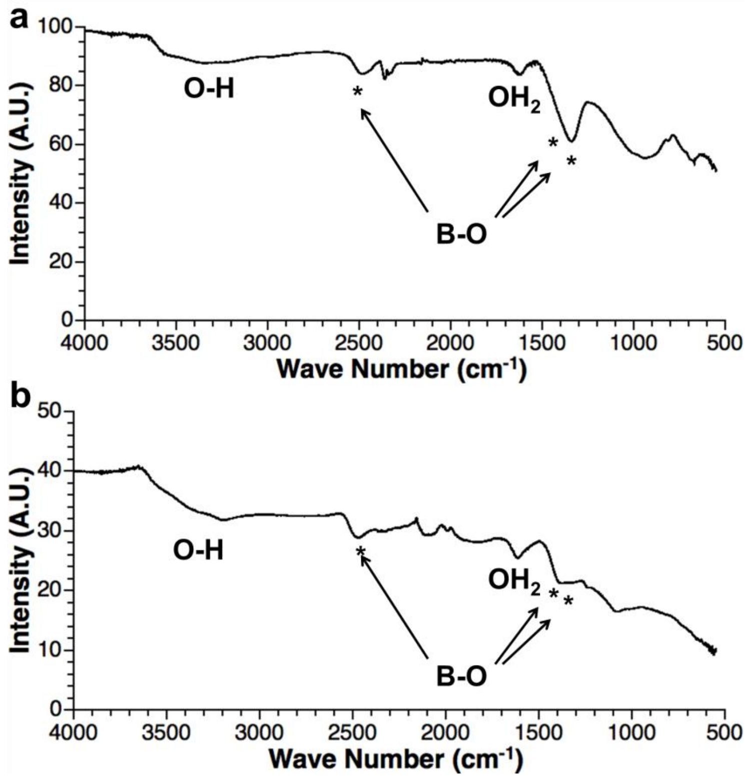


**Figure S1.** Fourier Transform Infrared spectra of (a) $HfB_2$/amorphous boron and (b) $CaB_6$/amorphous boron nanocomposites after exposure to air during seven days.

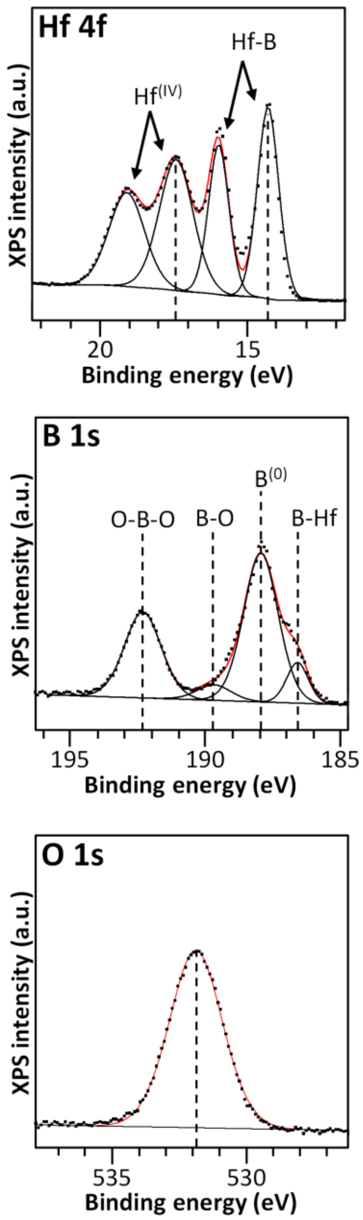


**Figure S2.** UHV-XPS spectra of the initial $HfB_2$ nanocomposite in the Hf $4f_{7/2}$, B 1s and O 1s regions. Incident photon energy : 1500 eV.

The composition of the superficial layer of the initial material was investigated using X-ray photoelectron spectroscopy under ultra-high vacuum (**Figure S2**). In the B 1s region, the signal reveals four distinct environments for boron. The most intense contribution is detected at a binding energy of 187.9 eV. It corresponds to elemental boron. The two peaks at higher binding energies of 190.0 and 192.4 eV are attributed to oxygen-bonded boron species. In comparison to the literature, they correspond to partially oxidized boron with one and two neighboring oxygen atoms, respectively.[1] These three species are attributed to the amorphous matrix, whereas the fourth one, detected at 186.6 eV, is attributed to boron included in $HfB_2$ nanocrystals.[2] The relatively low intensity of this peak is due to the metal boride being included in the amorphous matrix, *ca.* 3 nm deep. Indeed, B 1s electrons emitted deeply are partly reabsorbed by the material according to an exponential law. The depth of XPS analysis in each region can be evaluated by calculating the inelastic mean free path (IMFP) of electrons extracted with a given kinetic energy from a given material.[3] As the superficial layer is mainly composed of boron and oxygen, it is approximated to boron oxide for the calculations (considering only boron yields similar values). For incident photon energy of 1500 eV, the IMFP is 3.7 nm. It is thus expected that electrons emitted from $HfB_2$ are only partly detected. In the Hf 4f region, two distinct environments of hafnium are distinguished, each one being composed of two contributions due to the spin-orbit splitting of 1.7 eV between $4f_{7/2}$ and $4f_{5/2}$. The Hf $4f_{7/2}$ peak at 14.3 eV is attributed to hafnium at oxidation state (0)[4] and involved in $HfB_2$ in our case. The Hf $4f_{7/2}$ peak at 17.4 eV corresponds to $Hf^{(IV)}$.[4,5] It is attributed to oxidized hafnium in the superficial layer. A single contribution is detected in the O 1s region, at 531.9 eV. This is larger than the usual binding energy reported for oxygen in $HfO_2$ (530.2 eV)[5] and smaller than for B-O groups in $B_2O_3$ (533.2 eV).[6] It corresponds probably to hydroxyl groups Hf-OH reported at 531.7 eV [5] together with oxygen from B-O and O-B-O groups.


(1) Ennaceur, M. M.; Terreault, B. *J. Nucl. Mater.* **2000**, *280* (1), 33.

(2) Mavel, G.; Escard, J.; Costa, P.; Castaing, J. *Surf. Sci.* **1973**, *35*, 109.

(3) Tanuma, S.; Powell, C. J.; Penn, D. R. *Surf. Interface Anal.* **1994**, *21*, 165.

(4) Morant, C.; Galán, L.; Sanz, J. M. *Surf. Interface Anal.* **1990**, *16* (1-12), 304.

(5) Barreca, D.; Milanov, A.; Fischer, R. A.; Devi, A.; Tondello, E. *Surf. Sci. Spectra* **2007**, *14* (1), 34.

(6) Joyner, D. J.; Hercules, D. M. *J. Chem. Phys.* **1980**, *72* (2), 1095.

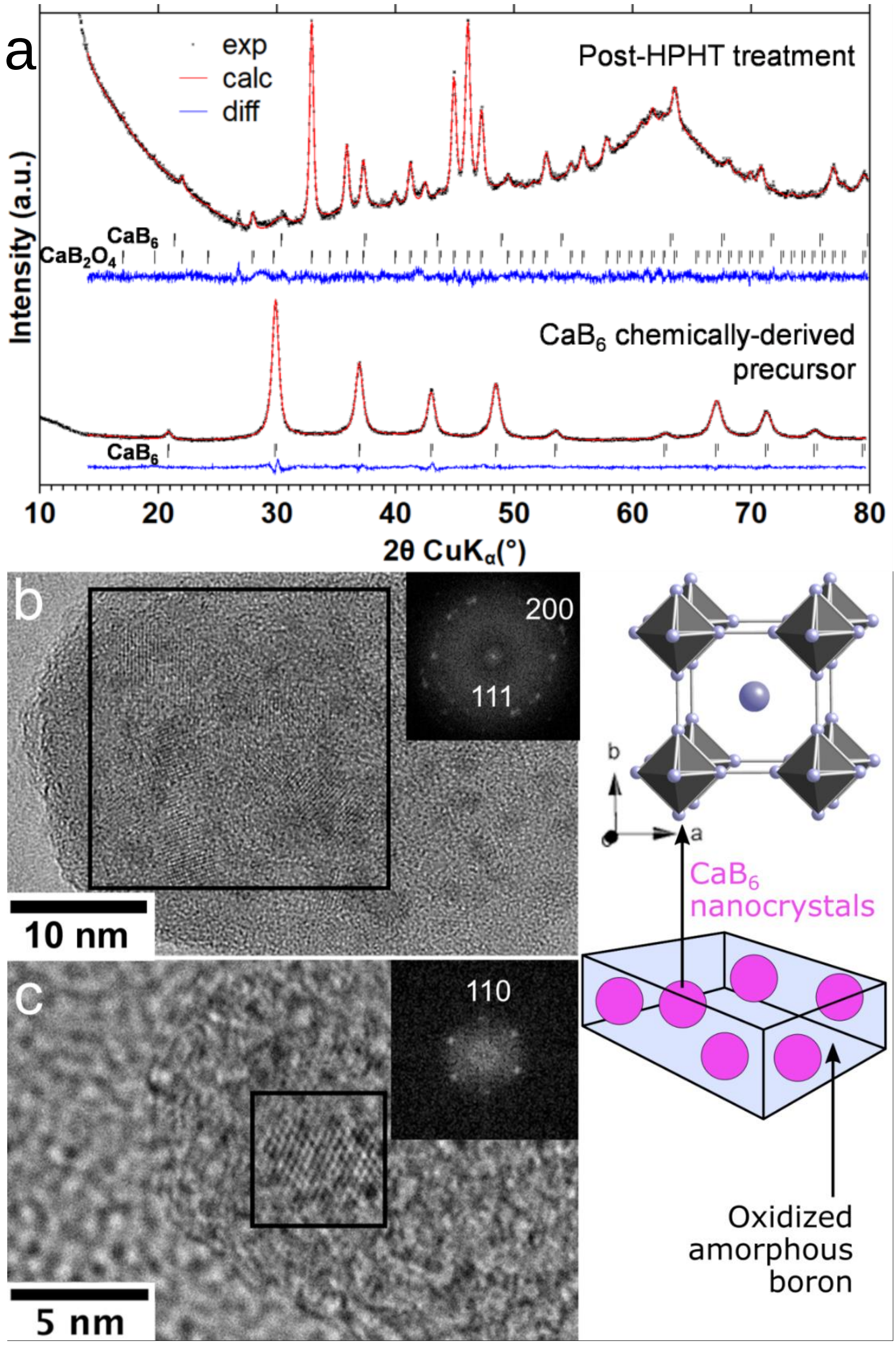


**Figure S3.** (a) XRD powder patterns of the initial $CaB_6$-based precursor and of the $CaB_6/CaB_2O_4$–(IV) nanocomposite obtained after treatment at 5 GPa and 1200 °C. For legibility sake, only main $CaB_2O_4$–(IV) peaks are indexed. $CaB_6$ peaks are highlighted as black triangles. (b) and (c) HRTEM images of the initial $CaB_6$-based precursor and corresponding FFTs of the black-squared zones, indexed along the $CaB_6$ structure. Scheme describing the initial material nanocomposite consisting in $CaB_6$ nanocrystals dispersed in an amorphous matrix composed of partly oxidized boron. ICSD reference cards are 196516 and 23241 for $CaB_6$ and $CaB_2O_4$ (IV), respectively. Refined cell parameters of $CaB_6$ and $CaB_2O_4$-(IV) were close to the values reported: a = 4.1565(6) Å for $CaB_6$ prior to any HP-HT treatment; a = 4.180(3) Å for $CaB_6$ and a = 9.0231(12) Å for $CaB_2O_4$ in the post-HP-HT samples.

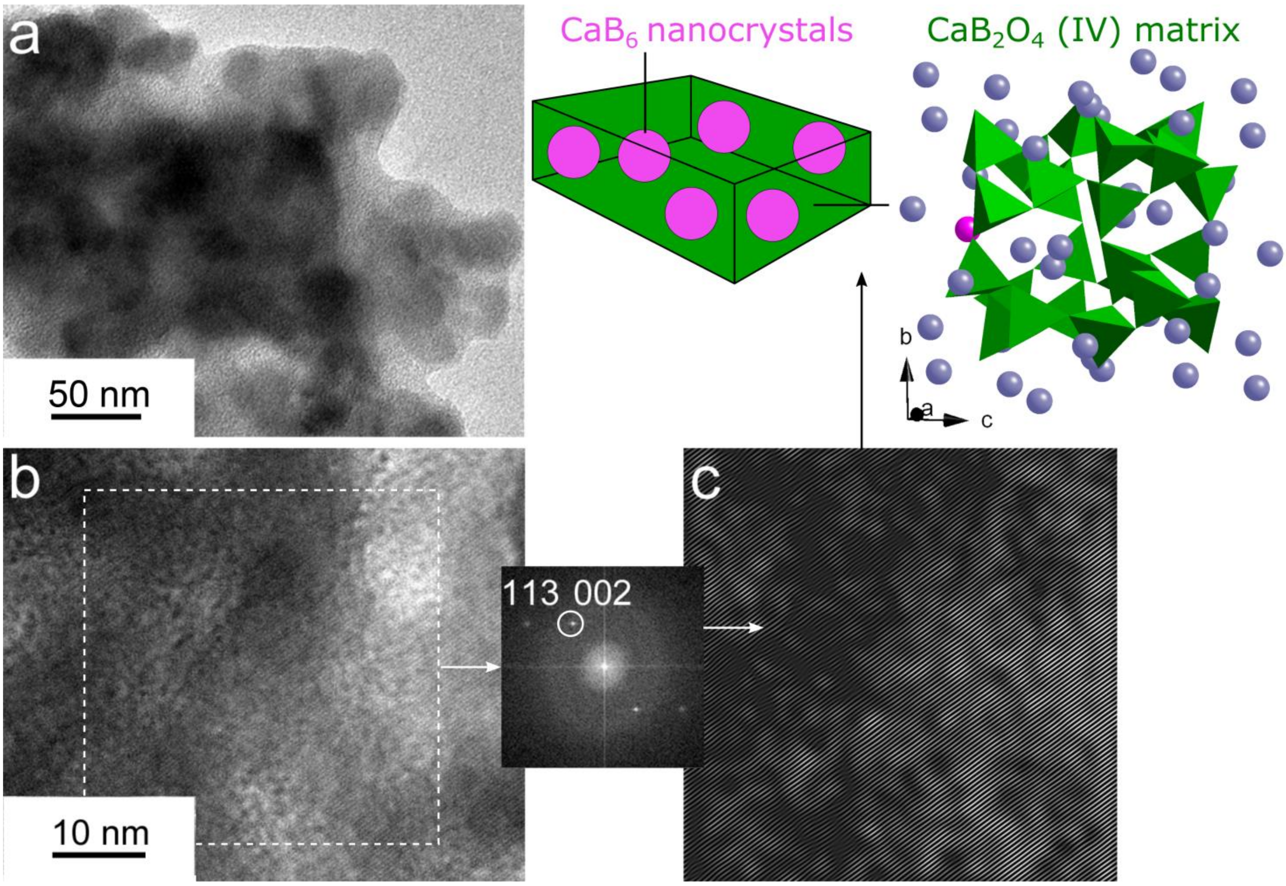


**Figure S4.** Transmission electron microscopy of the $CaB_6/CaB_2O_4$–(IV) nanocomposite obtained after HP-HT treatment: (a) TEM image showing the $CaB_6$ nanoparticles, (b) HRTEM image with FFT of the squared region and (c) corresponding $CaB_2O_4$–(IV) image Fourier-filtered from the (002) reflection, showing the extent of $CaB_2O_4$–(IV) matrix crystallization. Scheme of the nanocomposite obtained after HP-HT treatment, consisting in $CaB_6$ nanocrystals dispersed in a $CaB_2O_4$-(IV) matrix.